High frequency air monitoring by selected ion flow tube-mass spectrometry (SIFT-MS): influence of the matrix for simultaneous analysis of VOC, CO2, ozone and water

Mylène Ghislain, Nathalie Costarramone, Thierry Pigot, Marine Reyrolle, Sylvie Lacombe-Lhoste, Mickael Le Béchec

High frequency air monitoring by selected ion flow tube-mass spectrometry (SIFT-MS): influence of the matrix for simultaneous analysis of VOC, CO_2, ozone and water

Mylène Ghislain,[a,b] Nathalie Costarramone,[c] Thierry Pigot,[a] Marine Reyrolle,[a] Sylvie Lacombe,[a] Mickael Le Bechec[a]*

[a] CNRS / Universite de Pau et des Pays Adour/ E2S UPPA, IPREM, Institut des sciences analytiques et de Physicochimie pour l'environnement et les Matériaux, UMR5254, Hélioparc, 2 avenue Président Angot, 64053, PAU cedex 9, France

[b] Intersciences Nederlands, Tinstraat 16, 4823 AA Breda

[c] UT2A, 2 avenue Président Angot, 64053, PAU cedex 9, France

* Correspondence to : Mickael Le Bechec, CNRS/ Univ. Pau & Pays Adour/ E2S UPPA, IPREM, Institut des sciences analytiques et de Physicochimie pour l'environnement et les Matériaux, UMR5254, Hélioparc, 2 avenue Président Angot, 64053, PAU cedex 9, France

e-mail : mickael.lebechec@univ-pau.fr

Abstract

Selected Ion Flow Tube–Mass Spectrometry (SIFT-MS) with both positive (H_3O^+, $O_2^{\bullet+}$ and NO^+) and negative precursor ions ($O^{\bullet-}$, OH^-, $O_2^{\bullet-}$, NO_2^- and NO_3^-) was successfully used for the simultaneous monitoring at the ppbV level of VOC together with high CO_2, water or ozone concentration in complex matrixes. The use of negative precursor ions SIFT-MS allows the detection of carbon dioxide, water and ozone, while increasing the selectivity for VOC. The complete understanding of all the possible ion-molecule reactions led to the development of accurate quantification methods, independent of any variation of the air matrix composition. For instance, due to the low reactivity of carbon dioxide with OH^-, its correct monitoring implies considering not only the reaction of the analyte with the precursor ion, but also with their more reactive hydrates.

The results obtained by the developed method were validated on certified standard concentrations. This new SIFT-MS analysis method was further applied to an actual case for the evaluation of indoor air purifying devices and agreed with less convenient and more time-consuming standard analysis methods. It was thus demonstrated for the first time that the simultaneous high frequency, single run and direct monitoring of VOC, carbon dioxide, water and ozone gave a complete overview of the device operation and of the matrix evolution.

Keywords

Selected Ion Flow Tube – Mass Spectrometry; SIFT-MS; negative ionization; ion-molecule reaction; volatile organic compounds; VOCs; carbon dioxide, ozone, indoor air

Introduction

Nowadays, the monitoring of indoor air quality is an important challenge due to significant health, economic and societal issues related to indoor air pollution.[1] Indoor air quality is strongly affected by the presence of volatile organic compounds (VOC) such as aldehydes (mainly formaldehyde and acetaldehyde), or benzene, toluene, ethyl benzene and xylene (BTEX) among others.[2] Ozone, also found in indoor environment, is due to both outdoor-indoor air exchange and to air cleaning devices and imaging equipment.[3] Moreover, carbon dioxide, carbon monoxide and water are also present in indoor air.[1] Therefore, the development of a fast, accurate, and unique analysis method for the quantification of VOC at low concentration (ppbV range), CO_2 and ozone (in the ppbV to hundred ppmV range), as well as of water (in the tens g m^{-3} range for usual relative humidity) in complex air matrixes is of great interest.

Selected Ion Flow Tube–Mass Spectrometry (SIFT-MS) is a well-established direct injection mass spectrometry method for the direct and rapid analysis of VOC with typical detection limits ranging from parts-per-trillion (pptV) to parts-per-billion (ppbV) by volume in the gas phase depending on the instruments [4,5]. It is currently widely applied in the biological [6–8], medical [9–11], food [12–15] and environmental fields [16–19] because of its high frequency analysis rate and ease of use. In particular, the SIFT-MS technique appears to be a relevant method compared to chromatographic and/or derivatization methods for analysis of aldehydes and carboxylic acids in air.[20]

The SIFT-MS instrument is based on soft chemical ionization by precursor ions generated in a microwave-discharge plasma. Until recently, in SIFT-MS instruments, only positive ionization using H_3O^+, $O_2^{\bullet+}$ and NO^+ precursor ions was available. However, the recent development of a negative ionization source, using $O^{\bullet-}$, OH^-, $O_2^{\bullet-}$, NO_2^- and NO_3^- precursor ions, extended the range of analysable compounds and added a significant advantage in the discrimination of isobaric compounds. While methods using positive reagent ions may be used for the measurement of a large range of VOC [17,21–23], to the best of our knowledge, only few papers dealt with negative ionization SIFT-MS [20],[24]. An additional advantage of negative ionization SIFT-MS is the possibility to simultaneously monitor various compounds such as carbon dioxide and ozone together with various unreactive VOC by positive ionization.[20],[24] Thus, the combination of both the positive and negative ionization modes allows quantifying these compounds in complex mixtures. The analysis of carbon dioxide together with VOC is particularly relevant for such applications as indoor air quality, exhaled air analysis for health issues, headspace analysis of biological samples [11,25,26] or agri-food sector [27]. While CO_2 analysis reflects air containment and renewal in closed rooms, the simultaneous ozone quantification is also interesting for indoor air monitoring. For all these applications, the water content of air is most often greater than 40% relative humidity (RH). It was previously shown that water content of samples may influence the gas phase reactions involved in the flow tube of

positive ionization SIFT-MS and modify the quantification of some VOC.[28,29] This is due to the reactions between water and some precursor ions, and possibly with product ions, forming more or less reactive hydrates. Up to now, this analysis was not developed for negative ionization SIFT-MS. More generally, all the permanent components of air (water, oxygen, carbon dioxide, except nitrogen used as carrier gas), as well as ozone, might possibly also react in the flow tube with negative precursor ions.

Before performing the analysis of complex air mixtures by negative ionization SIFT-MS, it is thus necessary to fully understand the negative ions-water, -oxygen, -carbon dioxide, -ozone reactions in the flow tube. The present work aims at answering these questions (reactions mechanisms and experimental determination of their rate constants) and at applying the obtained results to a real case. Although some of these reactions were already investigated by SIFT-MS [30], the authors used a different carrier gas (He instead of N_2 in the present study), leading to different rate constants. In a second step, the efficiency of an air-cleaning device, claimed as providing ozone as a reactant, was analysed under EN 16846-1 standard conditions by positive and negative ionization SIFT-MS. Both VOC, carbon dioxide, water and ozone were simultaneously quantified at high frequency in a single run, with a systematic comparison of the data with conventional analysis methods.

Experimental

1 – SIFT-MS

A Voice 200 Ultra SIFT-MS (SYFT Technologies, Christchurch, New Zealand) equipped with a dual source producing positive and negative soft ionizing reagent ions (H_3O^+, NO^+, $O_2^{\bullet+}$, $O^{\bullet-}$, OH^-, $O_2^{\bullet-}$, NO_2^- and NO_3^-) in a single scan was used. The apparatus switches sequentially from the positive to the negative mode. The ions H_3O^+, NO^+, $O_2^{\bullet+}$, OH^-, $O_2^{\bullet-}$, are formed in water-containing plasma air (wet air), while the ions $O^{\bullet-}$, NO_2^- and NO_3^- are produced in dry plasma air. Precursor ions are generated by microwave discharge from air and water. Each precursor ion is sequentially selected by a first quadrupole mass filter and injected into the flow tube. The sample is introduced with the carrier gas (nitrogen, Air Liquide, Alphagaz 2) in the flow tube, maintained at 393K, through a heated inlet line (373K) with a flow rate of 20 mL min^{-1}. Product ions are analyzed by a second quadrupole mass filter.

For a reaction between a precursor ion R and an analyte A leading to the formation of a product ion P with a reaction rate constant *k*, the quantification of the analyte by SIFT-MS is simple and only requires the measurement of the precursor ion [R] and the product ions [P] count rates. In large excess of precursor ions (*i.e.* [R] >> [P]), the analyte number density into the flow tube [A] can be expressed:

$$[A] = \frac{[P]}{t_r k [R]} \qquad (A)$$

with t_r the reaction time in the flow tube and *k* the reaction rate constant. For simple two-body reactions k unit is in $cm^3\ s^{-1}$, while for three body reactions k_{3BD} unit is $cm^6\ s^{-1}$. In this

latter case, in order to calculate the effective binary rate constant k, k_{3BD} is multiplied by the carrier gas (nitrogen) number density in the flow tube.[31] In the present study, the experimental reaction rate constants of water, carbon dioxide and oxygen with positive and negative precursor ions were determined by introducing different C_{sample} of each individual compound in pure dry nitrogen (Air Liquide, Alphagaz 2).

The analyte sample concentration C_{sample} (in ppbV) is then obtained knowing the flow rates of the sample (Φ_s) and of the carrier gas (Φ_c), the flow tube temperature (T_{FT} , in Kelvin) and pressure (P_{FT} in Pa) as [22]:

$$C_{sample} = [A] \frac{k_B T_{FT} 10^{15}}{P_{FT}} \frac{(\Phi_s+\Phi_c)}{\Phi_s} \qquad \text{(B)}$$

with k_B the Boltzmann constant (m^2 kg s^{-2} $Kelvin^{-1}$).

2 – Gaseous atmospheres generation

The experiments with the permanent air components, water, oxygen and carbon dioxide, were carried out by adding known concentrations of each compound to pure dry nitrogen. The generation of these gas mixtures controlling the flow rate, the relative hygrometry and gases composition (N_2, O_2, CO_2) together with VOC was obtained with a device (Serv'Instrumentation, IRIGNY, France) equipped with three gas lines at different flow rates that merge together. Several gas tanks (Air liquid France Industrie, Paris, France)) containing pure and dry CO_2, O_2, or N_2, synthetic air (80% N_2, 20% O_2), diluted CO_2 (100 ppmV in N_2) and VOC mixture (1ppmV each of acetaldehyde, acetone, heptane and toluene in N_2) were used.

Ozone was produced with a Trailigaz L76 (Trailigaz bd de la Muette 95140 Gargès-lès-Gonesse) connected to dry synthetic air tank (80% N_2, 20% O_2). The O_3 flow rate was monitored with iodometric titration method [32]:–The dilution of O_3 was achieved by injecting a volume of ozone with tight gas syringes in a 13L dilution chamber previously flushed with the dilution matrix (Synthetic air or N_2 with controlled hygrometry).

3 – Evaluation of air purification devices

Three different commercial purification devices (named purifier A, purifier B and purifier C in the following) were evaluated. These three purifiers are equipped with HEPA and activated carbon filters. In addition to these filters, purifier A has a photocatalytic filter and a UV lamp, with optional generation of ozone. The evaluation of these air purifying devices involved the introduction (about 1 ppmV each) and analysis of five VOC representative of indoor air pollution with either the device OFF or ON in a 1.17 m^3 closed chamber according to the published CEN standard (EN 16846-1:2017)[33]. Acetaldehyde (≥99%), acetone (≥99%), *n*-heptane (≥99%), toluene (≥99%) and formaldehyde solution (37% wt. in water, containing 10-15% methanol as stabilizer) were supplied by Sigma-Aldrich (St. Louis, MO, USA). The air purifier was placed in the test chamber equipped with a

temperature and hygrometry probe (Testo 171, Forbach, France) and a fan (flow rate of 190 $m^3\ h^{-1}$). Humid clean air Zero (about 50% relative humidity) was supplied to the chamber by an air zero generator (F-DGS, Evry, France). Temperature was maintained at about 25°C. A mixture of the 5 VOC was injected in the chamber via a septum and, after concentration stabilization in the air chamber, the purifier was turned ON.[34] VOC, CO_2, ozone and water in the chamber were continuously monitored by SIFT-MS throughout the test using positive and negative ionization modes simultaneously. These data were compared to the results of conventional analysis methods. In parallel with the SIFT-MS measurements, acetone, heptane and toluene on the one hand, and carbon dioxide on the other hand, were automatically monitored by on-line gas chromatography (GC-FID for VOC and GC-methanizer-FID for CO_2 , Chromatotech, Saint Antoine, France) connected to the test chamber. Ozone concentrations were determined with Dräger sampling tubes (Dräger France SAS, Antony, France). Active sampling on cartridges impregnated with DNPH (2,4-dinitrophenylhydrazine) (Sigma-Aldrich, Saint Louis, MO, USA) followed by a solvent extraction prior to High Performance Liquid Chromatography (HPLC Infinity 1290 Agilent, Santa Clara, USA) analysis was used to control the concentrations of formaldehyde, acetaldehyde and acetone at the end of the test according to the NF ISO 16000-3 standard.

The analytical methods used for the monitoring of the studied compounds in comparison with the SIFT-MS technique are summarized in ESI, Table S1.

Results and discussion

1 – Relevant reactions in the flow tube

1.1 – Matrix-related reactions

Table 1 summarizes all the product ions arising from the flow tube reactions of water, oxygen and carbon dioxide with the eight positive and negative precursor ions.

Water reactions

When analyzing sampled air with usually high relative humidity by SIFT-MS, the knowledge and understanding of the reaction mechanisms between water and positive or negative precursors ions in the flow tube are essential. [28,29] The experimental reaction rate constants of water, carbon dioxide and oxygen with the various precursor ions were measured under our conditions and are summarized Table 2.

With H_3O^+ ion precursor, hydrated hydronium ions, $H_3O^+.(H_2O)_{1,2,3}$, with *m/z* of 37, 55 and 73, are produced via three-body reactions with N_2 as third body such as:

$$H_2O + H_3O^+ + N_2 \rightarrow H_3O^+.H_2O\ (m/z\ 37) + N_2 \qquad (1)$$

The formation of these water clusters with high signal intensity precludes any possibility of quantification of analytes that form product ions with *m/z* 37, 55 or 73 by reaction with H_3O^+. Furthermore, the reactions of $H_3O^+.(H_2O)_{1,2,3}$ hydrated ions with analytes may be significant and must be well known and considered for the analytes quantification.[28,29]

Water reacts much slower with NO^+ precursor ion to form $NO^+.H_2O$ cluster ion (*m/z* = 48) (Table 2), while no reaction occurs between water and O_2^+ precursor ion. Moreover $NO^+.H_2O$ ion is not very reactive compared to $H_3O^+.H_2O$ and does not form other hydrates. In negative ionization, no reaction is observed either with NO_2^- and NO_3^-, while the reaction with $O_2^{\bullet-}$ to form the monohydrate $O_2^{\bullet-}.H_2O$ ion (*m/z* = 50) is very slow. However, hydroxide (OH^-) and $O^{\bullet-}$ precursor ions react with water leading to $OH^-.(H_2O)_{1,2}$ cluster ions with *m/z* 35 and 53 in three-body association reactions [35] such as:

$$H_2O + OH^- + N_2 \rightarrow OH^-.H_2O\ (m/z\ 35) + N_2 \quad (2)$$

In the case of $O^{\bullet-}$ precursor ion, the presence of residual water in the flow tube leads to the formation of OH^- hydroxide ions. In addition to the primary reactions of the analyte with $O^{\bullet-}$ and OH^- ions, reactions with the very reactive cluster ions $OH^-.(H_2O)_{1,2}$ is observed.

.

Dioxygen reactions

No product ion from the reaction of dioxygen with the positive precursor ions is observed, contrary to the formation of several product ions with OH^-, $O^{\bullet-}$ and $O_2^{\bullet-}$ negative precursors ions. The reaction of dioxygen with OH^- or $O^{\bullet-}$, in the absence or presence of water and carbon dioxide, leads to two products ions at *m/z* 32 and 48 (Eqs. 3a-b and 4a-b), with significantly different 32/48 ratios (Table 2):

$$OH^- + O_2 \rightarrow O_2^{\bullet-}\ (m/z\ 32\ ,93\%) + OH^{\bullet} \quad (3a)$$

$$\rightarrow O_3^{\bullet-}\ (m/z\ 48,7\%) + H^{\bullet} \quad (3b)$$

$$O^{\bullet-} + O_2 \rightarrow O_2^{\bullet-}\ (m/z\ 32,13\%) + O^{\bullet} \quad (4a)$$

$$\rightarrow O_3^{\bullet-}\ (m/z\ 48,87\%) \quad (4b)$$

With $O_2^{\bullet-}$ as precursor ion, the sole $O_3^{\bullet-}$ product ion at m/z 48 is observed, since *m/z* 32 corresponds to the precursor ion itself.

Carbon dioxide reactions

Although carbon dioxide is unreactive with positive precursor ions, CO_2 produces new product ions by reaction with negative precursors with a significant signal intensity due to the high level of CO_2 concentrations in air (in the order of tens/hundreds ppmV).

The reaction between CO_2 and OH^- leads mainly to the formation of the *m/z* 61 (HCO_3^-) ion with increasing intensity with increased CO_2 concentration in the flow tube (ESI, Figure S1). This observation is consistent with Eq. 5, a three-body association with N_2 as third body, in agreement with the literature [35]:

$$OH^- + CO_2 + N_2 \rightarrow HCO_3^-\ (m/z\ 61) + N_2 \quad (5)$$

Under our experimental conditions, the three-body rate constant is determined to be 2.49 10^{-28} cm^6 s^{-1} corresponding to an effective bimolecular rate constant of 2.92 10^{-12} cm^3 s^{-1} (Table 2). This reaction is slow compared to the reaction of OH^- with the previously selected VOC (see section 1.2) and its rate constant is of the same order of magnitude as that of OH^- with water (Table 2). Isotopic ions at *m/z* 62 and 63 (proportional signals to that of HCO_3^-) are also detected, corresponding to $H^{13}CO_3^-$ (*m/z* 62), $HC^{17}O^{16}O_2^-$ (*m/z* 62) or $HC^{18}O^{16}O_2^-$ (*m/z* 63). Although insignificant for quantification, these ions may be potential interferent at *m/z* of 62 and 63. It is important to notice that the signal at *m/z* 61 (HCO_3^- ion) increases with increasing water amount (ESI, Figure S2). This implies that the reaction of CO_2 with OH^- monohydrate, $OH^-.H_2O$, also leads to the formation of HCO_3^- and of its hydrates according to the following reaction (Eq. 6):

$$OH^-.H_2O + CO_2 + N_2 \rightarrow HCO_3^- (m/z\ 61) + H_2O + N_2 \qquad (6)$$

This already reported reaction [36] is much faster (effective bimolecular rate constant *k* = 2.63 10^{-9} cm^3 s^{-1} than the direct reaction (Eq. 5) with OH^- precursor ion (*k* = 2.92 10^{-12} cm^3 s^{-1}, Table 1) and represents a significant pathway of HCO_3^- ion production in the presence of water.

The formation of product ions at *m/z* of 79, 97 and 115 (ESI, Figure S2), corresponding to HCO_3^- hydrates (Eqs. 7a-c), are also observed experimentally in the presence of water in the flow tube. These hydrates can arise from the secondary reaction between HCO_3^- product ion and H_2O:

$$HCO_3^- + H_2O \rightarrow HCO_3^-.H_2O\ (m/z\ 79) \qquad (7a)$$

$$HCO_3^-.H_2O + H_2O \rightarrow HCO_3^-.(H_2O)_2\ (m/z\ 97) \qquad (7b)$$

$$HCO_3^-.(H_2O)_2 + H_2O \rightarrow HCO_3^-.(H_2O)_3\ (m/z\ 115) \qquad (7c)$$

but also from the reaction of OH^- hydrates, $OH^-(H_2O)_n$ already noticed as reaction products (Eq. 2) between water and OH^- with CO_2 (Eq. 8) [35]:

$$OH^-.(H_2O)_n + CO_2 + N_2 \rightarrow HCO_3^-.(H_2O)_n + N_2 \qquad (8)$$

In any case, HCO_3^- hydrates cannot be neglected and must be considered for CO_2 determination.

The reactions of CO_2 with dioxygen product ions such as $O_2^{\bullet -}$ and $O_3^{\bullet -}$ from Eqs. 3 and 4 a-b have also to be considered as shown by the product ions at m/z 76 and 60 in Table 1:

$$O_2^{\bullet -} + CO_2 \rightarrow CO_2.O_2^{\bullet -}\ (m/z\ 76) \qquad (9)$$

$$O_3^{\bullet -} + CO_2 \rightarrow CO_2.O^{\bullet -}(m/z\ 60) + O_2 \qquad (10)$$

Actually, dioxygen also influences the analysis of CO_2 but less critically than water since O_2 concentration is generally constant relative to humidity between air samplings. Figure 1 summarizes all the different reactions of CO_2 with the other matrix ion products.

With $O^{\bullet-}$ precursor ion, the formation of OH^- ion from reaction between $O^{\bullet-}$ and water is dominating in the flow tube. In addition to reactions with OH^- ion (Eqs. 4 to 10), CO_2 reacts directly with $O^{\bullet-}$ ion precursor leading to $CO_2.O^{\bullet-}$ ion at *m/z* 60.

Reactions with $O_2^{\bullet-}$ precursor ion are much simpler with only two product ions: at *m/z* 76 ($CO_2.O_2^{\bullet-}$) either from the direct reaction with the precursor (Eq. 9) or with $O_2^{\bullet-}$ hydrate, $O_2^-.H_2O$ (Eq. 11), and *m/z* = 60 ($CO_2.O^{\bullet-}$) from the reaction with the dioxygen product ion $O_3^{\bullet-}$ leading to $CO_2.O^{\bullet-}$ (Eq. 10). (ESI, Figure S3).

$$O_2^{\bullet-}.H_2O + CO_2 \rightarrow CO_2.O_2^{\bullet-}\ (m/z\ 76) + H_2O \qquad (11)$$

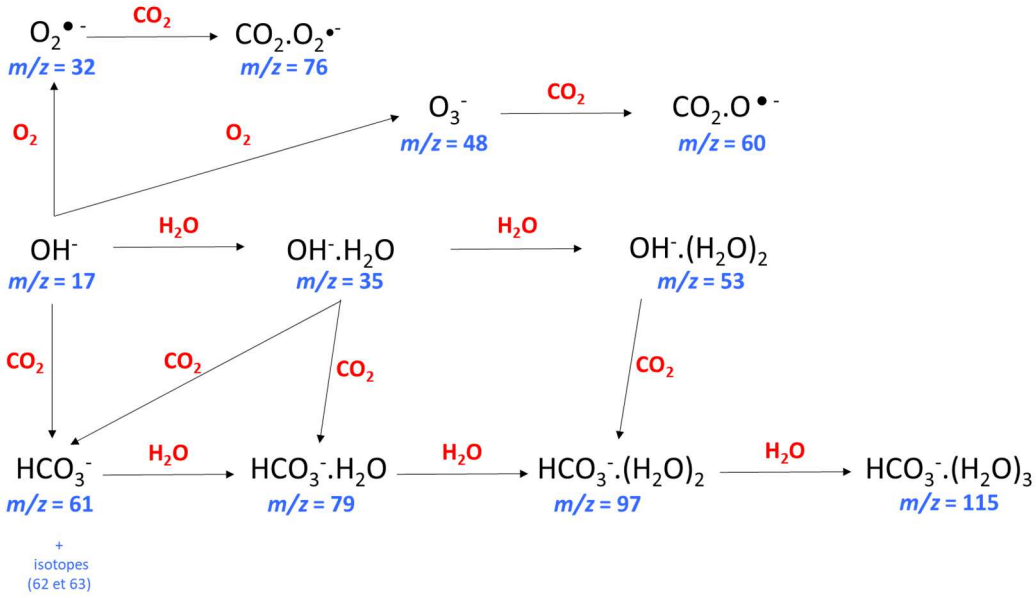

Figure 1. Reactions of water, oxygen and carbon dioxide in the flow tube with OH^- precursor ion.

From Tables 1 and 2, it appears that the permanent air matrix components are more reactive with the negative precursor ions (except NO_2^- and NO_3^-) than with the positive ones, since only water reacts with H_3O^+ leading to $H_3O^+.(H_2O)_n$ product ions, with three important consequences:

- The corresponding ions add up 3 possible interferents at *m/z* 37 ($H_3O^+.H_2O$), *m/z* 55 ($H_3O^+.(H_2O)_2$) and *m/z* 73 ($H_3O^+.(H_2O)_3$).
- Since the hydrate product ions are also reactive, they can act as new precursor ions.
- A high depletion of precursors ions (H_3O^+) may be observed since water concentration can be very high in actual air samples (at g m^{-3} level).

Similarly, OH^-, $O_2^{\bullet-}$ and the most reactive $O^{\bullet-}$ ions mainly react with water, but also with dioxygen and carbon dioxide leading to negative product ions with possible interferences, new reactivity and precursor depletion. These issues were considered in the following quantification of VOC in air matrixes.

1.2 – VOC reactions

Five VOC characteristic of indoor air pollution (formaldehyde, acetaldehyde, acetone, toluene and heptane) [33] were reacted in the flow tube with positive and negative precursor ions under various conditions. In pure nitrogen (N_2) matrix, their reactions with the different precursor ions are quite simple and generally lead to the formation of single primary product ions, well known in the case of positive precursors [22,25,28,37] (Table 3). The reactions of H_3O^+ with the studied compounds are exclusively exothermic proton transfer with the formation of AH^+ ions as with acetone for instance (Eq. 12):

$$H_3O^+ + CH_3COCH_3 \rightarrow CH_3COCH_3H^+ (m/z\ 59) + H_2O \quad (12)$$

Secondary association reactions between these primary ions and neutral analyte molecules may occur in the flow tube leading to the formation of $A.AH^+$ dimer ions. This is the case of aldehydes and acetone with the formation of $CH_3COCH_3.CH_3COCH_3H^+$ (m/z 117) and $CH_3COCH_3H^+.H_2O$ (m/z 77) ions for instance in the latter case (Table 3).

In the presence of water, secondary ions corresponding to hydrates of primary ions ($AH^+.H_2O$) are observed (Eq. 13):

$$AH^+ + H_2O \rightarrow AH^+.H_2O \quad (13)$$

Furthermore, hydrated precursor ions $H_3O^+.H_2O$ (from Eq. 1) are reactive and can act as new precursors giving rise to hydrated protonated ions $AH^+.H_2O$ via ligand switching reaction (Eq. 14) [38]:

$$H_3O^+.H_2O + A \rightarrow AH^+.H_2O + H_2O \quad (14)$$

With the NO^+ reagent ion, three main reactions occur (Table 3), without any secondary reaction when adding water, dioxygen and/or carbon dioxide:

- A three-body ion-molecule association leading to the formation of $A.NO^+$ product ions, as for instance between acetone and NO^+ and N_2 ($CH_3COCH_3.NO^+$ *m/z* = 88).
- Hydride ion transfer gives $(A\text{-}H)^+$ ions, as shown with acetaldehyde (CH_2CHO^+ *m/z* = 43).
- Charge transfer forming $A^{+\bullet}$ product ions as with toluene with $C_7H_8^+$ *m/z* = 92 as single product ion.

With the $O_2^{\bullet+}$ reagent ion, charge transfer to give $A^{\bullet+}$ also occurs with four VOC, except heptane. Reactions with $O_2^{\bullet+}$ can also proceed via dissociative charge transfer resulting in different fragment ions, as with heptane as a typical example, which gives two different fragment ions in addition to the charge transfer ion $C_7H_{16}^{+\bullet}$ at m/z 100: $C_5H_{11}^+$ (*m/z* = 71) and $C_4H_9^+$ (*m/z* = 57). As with the H_3O^+ reagent ion, $A.AH^+$ secondary cluster ions can be produced via the reaction between the primary product ions and neutral molecules of analytes as for instance $CH_3CHO.CH_3CHOH^+$ (m/z 89) from acetaldehyde.

Proton abstraction by the OH^-, $O^{\bullet-}$ and $O_2^{\bullet-}$ reagent ions was experimentally shown in a previous work [20] to be the single reaction pathway for aldehydes, according to Eq. 15. Energy calculations demonstrated that hydrogen abstraction by OH^- occurred from the CH_x group alpha to the carbonyl group.

$$OH^- + A \rightarrow (A-H)^- + H_2O \quad (15)$$

Proton abstraction is also the main reaction pathway in the case of acetone and toluene (Table 3), while heptane does not react with any of the five negative ions. No reaction was observed between aldehydes or acetone and either NO_2^- or NO_3^-.

As with H_3O^+, the presence of water has a strong influence on the reactivity in the flow tube with OH^-, $O^{\bullet-}$ and $O_2^{\bullet-}$. $(A-H)^-.H_2O$ secondary ions can be formed from three-body association between $(A-H)^-$ primary product ions and water molecules (Eq. 16):

$$(A-H)^- + H_2O + N_2 \rightarrow (A-H)^-.H_2O + N_2 \quad (16)$$

Reactions between the analyte and the monohydrate precursor ion $OH^-.H_2O$ may also lead to either $(A-H)^-.H_2O$ (Eq. 17) or to $(A-H)^-$ (Eq. 18):

$$A + OH^-.H_2O \rightarrow (A-H)^-.H_2O + H_2O \quad (17)$$

$$A + OH^-.H_2O \rightarrow (A-H)^- + 2H_2O \quad (18)$$

In this case, $(A-H)^-$ ions can arise from either Eq. 15 or Eq. 18 with potentially different reaction rate constants, as illustrated in Figure 2 depicting the reactions between acetone and OH^- as precursor ion. This will imply several consequences for the quantification. First, the $(A-H)^-.H_2O$ hydrate product ions must be considered and their count rate included in the quantification in addition to the count rate of the primary product ions $(A-H)^-$. Second, the $OH^-.H_2O$ ion must be considered as a precursor ion in addition to OH^-, since it is in large excess in the flow tube ($[OH^-.H_2O] >> [(A-H)^-] + [(A-H)^-.H_2O]$) and is invariant with time during the reaction.

No additional reactions were observed in the presence of CO_2 and/or O_2 in the matrix, even if these molecules can produce possible interferences: for example, acetaldehyde and CO_2 both give product ions at *m/z* = 61 by reaction with OH^- and $O^{\bullet-}$, but not with $O_2^{\bullet-}$.

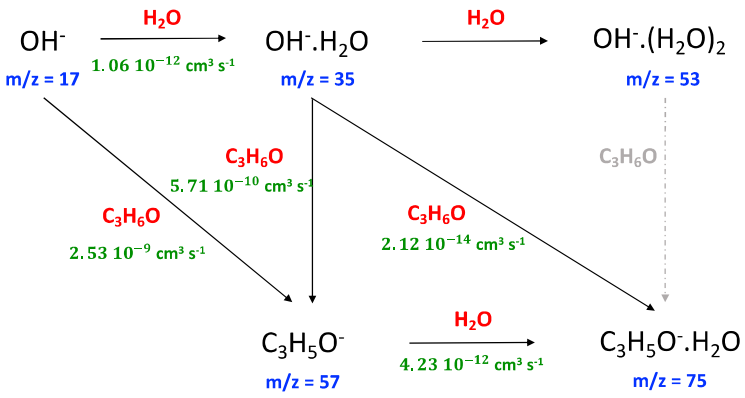

Figure 2. Reactions and experimental rate constants in the flow tube between acetone and OH^- ion precursor ion.

1.3 – Ozone reactions

In a pure nitrogen matrix, ozone reacts by charge transfer with OH^-, $O^{\bullet-}$ and $O_2^{\bullet-}$ negative precursor ions to form $O_3^{\bullet-}$ (*m/z* = 48) product ions (Eq. 19):

$$OH^- + O_3 \rightarrow O_3^{\bullet-}\ (m/z\ 48) + OH^{\bullet} \quad (19)$$

Since $O_3^{\bullet-}$ ion is also detected (Eqs. 3b and 4b) when analyzing dioxygen alone, an interference is expected between ozone and dioxygen of the matrix when using OH^-, $O^{\bullet-}$ and $O_2^{\bullet-}$, as illustrated in ESI, Figure S4. In a matrix containing CO_2, reaction between $O_3^{\bullet-}$ and CO_2 lead to the formation of $CO_2.O^{\bullet-}$ (m/z = 60) according to Eq. 10. Although it was previously reported that ozone in the hundreds of ppmV range also reacts with NO_2^- (rate constant about 1.7 10^{-10} cm^3 s^{-1}), in the ppbV range of the present study, the product ion concentrations are too low for ozone quantification using the OH^- reagent ion. [27]

Although the reaction mechanisms of ozone in the flow tube are quite simple with few different product ions, the interferences with the air matrix must be considered for the analysis of ozone by negatively charged SIFT-MS reagent ions.

2 – SIFT-MS quantification

2.1 - Water

The reaction of water with the NO^+ reagent ion is simple with only one product ion $NO^+.H_2O$ (Table 1, section 1.1) and relatively slow (k = 6.08 10^{-13} cm^3 s^{-1}, Table 2) compared to the H_3O^+ and OH^- reagent ions (k = 7.16 10^{-11} and 1.06 10^{-12} cm^3 s^{-1}, Table 2), but fast enough allowing a good quantification of water according to Eq. C:

$$[H_2O]_{\text{flow tube}} = \frac{[NO^+.H_2O]}{t\,[NO^+]\,k_{NO^+}} = \frac{[48]}{t\,[30]k_{NO^+}} \quad (C)$$

Due to the small reaction rate constant, NO^+ ions are poorly consumed and remain in a very large excess compared to the $NO^+.H_2O$ product ions even with high water concentrations in air. Thus, the NO^+ reagent ion seems suitable for an accurate quantification of water (Figure 4).

On the other hand, in a previous paper, Španěl and Smith measured the amount of water in an air sample by SIFT-MS by monitoring the count rate of $H_3O^+.(H_2O)_{1,2,3}$ product ions from Eq. 1 and the count rate of H_3O^+ precursor ions. Water was then considered as an analyte and quantified according to Eq. D [31]:

$$[H_2O]_{\text{flow tube}} = \frac{[H_3O^+.H_2O]+[H_3O^+.(H_2O)_2]+[H_3O^+.(H_2O)_3]}{t\,[H_3O^+]\,k_{H_3O^+}} = \frac{[37]+[55]+[73]}{t\,[19]\,k_{H_3O^+}} \quad (D)$$

Reaction of Eq. 1 leading to hydrated hydronium ions, $H_3O^+.H_2O$, is fast (k = 7.16 10^{-11} cm^3 s^{-1}, Table 2). Consequently, high water level can lead to a significant depletion of the H_3O^+ precursor ion in the flow tube, since $H_3O^+.(H_2O)_{1,2,3}$ are formed with $[H_3O^+.H_2O]$ + $[H_3O^+.(H_2O)_2]$ + $[H_3O^+.(H_2O)_3]$ > $[H_3O^+]$ as already highlighted by Španěl [28]. In practice, in case of large amount of water, due to its high reactivity with H_3O^+ , the precursor ion is no longer in excess. This leads to an underestimation of the concentration of water as shown

Figure 3 where the slope of the correlation line between the measured and the theoretical water concentration is 0.92 when using H_3O^+ *vs* 1.00 with NO^+ precursor ion.

Similarly, because of the high level of water concentration in air and the high rate constant between water and the OH^- reagent ion (k = 1.06 10^{-12} cm^3 s^{-1}, Table 2), the same reasoning as with the H_3O^+ reagent ion holds true. According to Eq. 2, the amount of water can be determined by Eq. E:

$$[H_2O]_{\text{flow tube}} = \frac{[OH^-.H_2O]+[OH^-.(H_2O)_2]}{t\,([OH^-]\,k_{OH^-})} = \frac{[35]+[53]}{t\,([17]\,k_{OH^-})} \qquad \text{(E)}$$

Depletion of the OH^- precursor ion by water is also an issue, but to a lesser extent than with H_3O^+ since $k_{H_3O^+} > k_{OH^-}$, with the slope of the correlation line between the measured and the theoretical water concentration equal to 0.93 (Figure 3).

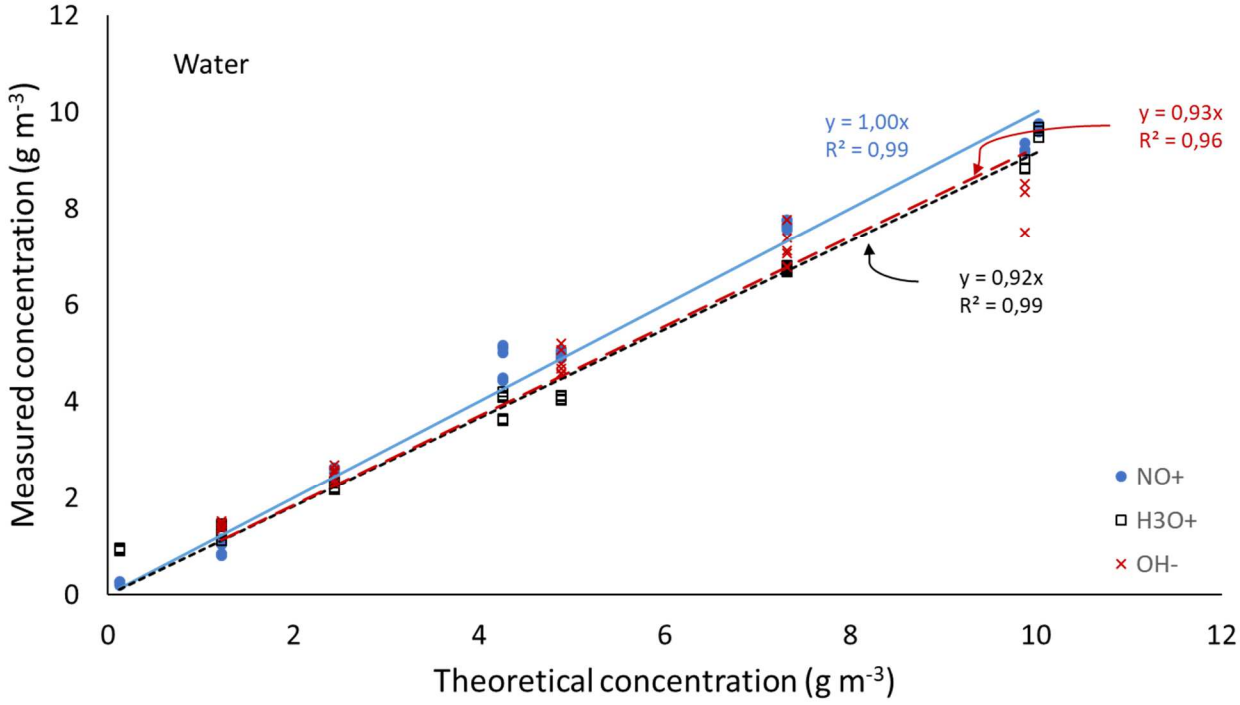

Figure 3. Water quantification in air by SIFT-MS with NO^+, H_3O^+ and OH^- precursor ions.

Consequently, for SIFT-MS quantification of analytes in a water-rich matrix, a careful attention must be paid on [P]/[R] ratio when using H_3O^+ and OH^- precursor ions, while the results are more reliable with NO^+ ion.

2.2 – CO_2

Quantification of CO_2 is only possible with negative precursor ions because it does not react with H_3O^+, NO^+ or $O_2^{\bullet+}$. The reactions with OH^-, $O^{\bullet-}$ and $O_2^{\bullet-}$ are fast enough to quantify CO_2 in air because of its high levels of concentration (in the order of tens/hundreds ppm).

As detailed in section 1.1, reactions of CO_2 in the flow tube using OH^- as precursor ion lead to several product ions: the primary product ion HCO_3^-at *m/z* = 61 (major ion, Eq. 5), its hydrates $HCO_3^-.(H_2O)_n$ with *m/z* 79, 97 and 115 (Eqs. 7a-c), and the ions resulting from the reactions with $O_2^{\bullet-}$ and $O_3^{\bullet-}$ (product ions from the reactions between OH^- and dioxygen, Eq. 3a-b), $CO_2.O^{\bullet-}$ at *m/z* = 60 and $CO_2.O_2^{\bullet-}$ 76 (Eqs. 9 and 10). The reaction between CO_2 and $O_2^{\bullet-}$ is slow with a rate constant k =2.63 10^{-13} cm^{-3} s^{-1}, about 10 times lower than the reaction of CO_2 with OH^- (2.92 10^{-12} cm^{-3} s^{-1}, Table 1). However, all the other product ions from CO_2 must be considered for an accurate quantification.

It is important to remember that the reaction rate constant of CO_2 with the $OH^-.H_2O$ hydrate (m/z 35, Eq. 8) is higher than that of the reaction with the OH^- reagent ion (three-body association rate constant, k_{3BD} = 2.2 10^{-25} versus 2.5 10^{-28} cm^6 s^{-1}). Thus, the $OH^-.H_2O$ hydrate ion acts as a precursor and this reaction must also be considered in the calculation of the CO_2 concentration. This implies that the $OH^-.H_2O$ hydrate ions and the OH^- precursor ions must be in large excess relative to the product ions (Eqs. F and G):

$$([OH^-.H_2O] \gg [HCO_3^-] + [H^{13}CO_3^-] + [HC^{17}O^{16}O_2^-] + [HC^{18}O^{16}O_2^-] + [HCO_3^-.H_2O] + [HCO_3^-.(H_2O)_2] + [HCO_3^-.(H_2O)_3]) \quad (F)$$

$$([OH^-] \gg [HCO_3^-] + [HC^{17}O^{16}O_2^-] + [HC^{18}O^{16}O_2^-] + [HCO_3^-.H_2O] + [HCO_3^-.(H_2O)_2] + [HCO_3^-.(H_2O)_3]) \quad (G)$$

The relative number densities (molecules cm^{-3}) of $OH^-.(H_2O)_{1,2,3}$ are not constant along the reaction tube since water is introduced in the flow tube together with the sample via the sampling line, unlike the OH^- precursor ions injected at the inlet of the flow tube. Thus, as already proposed by Španěl, the proportion of hydrated hydroxide ions can be considered as halves of their downstream count rate [28]. The calculation of the CO_2 concentration in the flow tube relies thus on Figure 1 leading to Eq. H:

$$[CO_2]_{\text{flow tube}} = \frac{[HCO_3^-] + [H^{13}CO_3^-] + [HC^{17}O^{16}O_2^-] + [HC^{18}O^{16}O_2^-] + [HCO_3^-.H_2O] + [HCO_3^-.(H_2O)_2] + [HCO_3^-.(H_2O)_3]}{t\left([OH^-]k_{17} + [OH^-.H_2O]\frac{k_{35}+k_{17}}{2}\right)}$$

$$[CO_2]_{\text{flow tube}} = \frac{[61]+[62]+[63]+[79]+[97]+[115]}{t([17]k_{17}+[35]\frac{k_{35}+k_{17}}{2})} \quad (H)$$

with k_{17} and k_{35}, the reaction rate constants between CO_2 and OH^- or $OH^-.H_2O$ respectively (2.92 10^{-12} and 2.63 10^{-9} cm^3 s^{-1}).

Figure 4 compares the CO_2 concentration calculated with Eq. A considering only the primary reaction between OH^- and CO_2 and with Eq. H, considering all the reactions related to the presence of water in the matrix (Eqs. 6-8). It is obvious that it is impossible to quantify correctly CO_2 without including $HCO_3^-.(H_2O)_n$ hydrates as product ions and $OH^-.H_2O$ as a hydrated precursor ion, except if CO_2 concentration is high relative to water concentration. This result accounts for the previous literature data where different product ions ($CO_2.O_2^{\bullet-}$ and $CO_2.O^{\bullet-}$) were used depending on CO_2 concentration.[24]

As recalled in the previous section, the reactions of CO_2 with $O^{\bullet-}$ are still more complex and cannot be used easily for an accurate determination of CO_2 concentration. As well, the CO_2/

$O_2^{\bullet-}$ reaction (Eq. 9) is not considered due to its low rate constant (k = 2.63 10^{-13} cm^3 s^{-1}, Table 2) and to the slow production of $O_2^{\bullet-}.H_2O$ (Eq. 11, k = 7.73 10^{-13} cm^3 s^{-1}).

2.3 – VOC

With either H_3O^+ or OH^- and $O^{\bullet-}$, the production of reactive hydrates has to be considered, but their reaction rate constants with VOC are low (see Figure 2, example of acetone). Accordingly, their influence on the calculation of VOC concentrations are poor and do not require any correction, as shown with acetone and toluene using OH^- precursor ion in Figure 4. With H_3O^+, Španěl *et al.* previously showed that the highest deviation between theoretical and measured acetone concentration was within 13% at the highest water concentration.[28] The already noted interference at *m/z* = 61 between $CH_2CHO^-.H_2O$ and HCO_3^- precludes acetaldehyde quantification at low concentration with either OH^- or $O^{\bullet-}$, even it is should be possible with $O_2^{\bullet-}$ in spite of rather low reaction rate constant (k = 9 10^{-11} cm^3 s^{-1}).[20]

2.4 – Ozone

Ozone was shown to react with OH^-, $O^{\bullet-}$ and $O_2^{\bullet-}$ to produce $O_3^{\bullet-}$ (Eq. 19). But $O_3^{\bullet-}$ can also arise from the reaction OH^- or $O^{\bullet-}$ with O_2 (Eqs 3b, 4b and ESI, Figure S4). In addition $O_3^{\bullet-}$ also further reacts with CO_2 from the matrix (Eq. 10). Under these conditions, it is however possible to determine its concentration according to Eq. I using the OH^- reagent ion:

$$[O_3]_{flow\ tube} = \frac{([O_3^{\bullet-}] + [CO_2.O^{\bullet-}]) - ([O_3^{\bullet-}] + [CO_2.O^{\bullet-}])_{matrix}}{t[OH^-]k_{17}} = \frac{([48]+[60]) - ([48]+[60])_{matrix}}{t[17]k_{17}} \qquad (I)$$

The $([48] + [60])_{matrix}$ count rate may be obtained from a blank measurement, but neglecting any variation of oxygen concentration between the blank and the sample. Alternatively, according to Eq. 3a, 3b and 10, it is possible to estimate the $([48]+[60])_{matrix}$ as 7% of the measured oxygen concentration in the matrix.

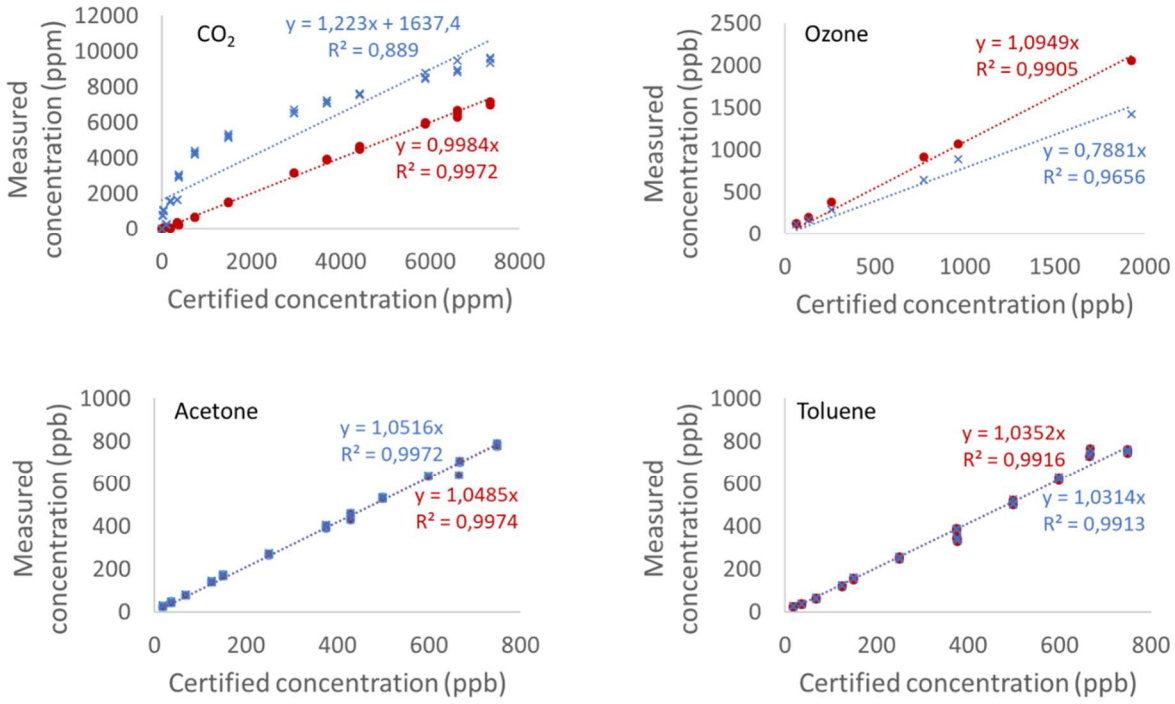

Figure 4. Influence of water on VOC, CO_2 and ozone quantification in humid air (N_2/O_2 (80/20), 40% RH) by SIFT-MS negative ionization (OH^- precursor). Measured concentrations obtained with simple calculation using product ions/precursor ion ratio according to eq. A (x) and measured concentrations obtained considering secondary product ions with water and water clusters according to Eq. H to I (●).

2.5 – Validation of SIFT-MS quantification

The concentrations of 4 VOCs and of CO_2 from certified standard gas tanks determined with the above-mentioned SIFT-MS calculations (ions used detailed in ESI, Table S1) were compared to the concentrations obtained with more conventional GC-FID and GC-FID/methanizer analysis (ESI, Table S2). The SIFT-MS method gives satisfactory slightly over-estimated VOCs concentrations. When applying Eq. H. for the calculation of CO_2 concentrations, quite reliable results are obtained. In particular, in the lowest concentration range, the SIFT-MS method for CO_2 is more accurate than the GC-FID analysis.

The limit of detection (LOD, ESI Table S1) of the SIFT-MS method is higher than that of DNPH/HPLC methods for aldehydes, but much lower than that of on-line GC-FID for the other VOCs.

3 – Application to a real case: evaluation of air purifying devices by simultaneous monitoring of VOC, CO_2, ozone and water in air

The negative and positive SIFT-MS analysis method was further applied to the evaluation of three air purifying devices, by simultaneously measuring VOC, CO_2, ozone (only available with device A) and water in a large volume chamber with the device on and off

according to EN 16846-1standard.[33,34] The ions used for SIFT-MS analysis considering all the possible interferences are summarized in ESI, Table S1. The complete monitoring of each compound with time for device A is described in ESI, Figure S5 for VOC and Figure 5 for CO_2, ozone and water. Formaldehyde, acetaldehyde and acetone concentrations, measured by SIFT-MS and HPLC analysis at the end of the purifying step are compared for the three devices in ESI Table S3.

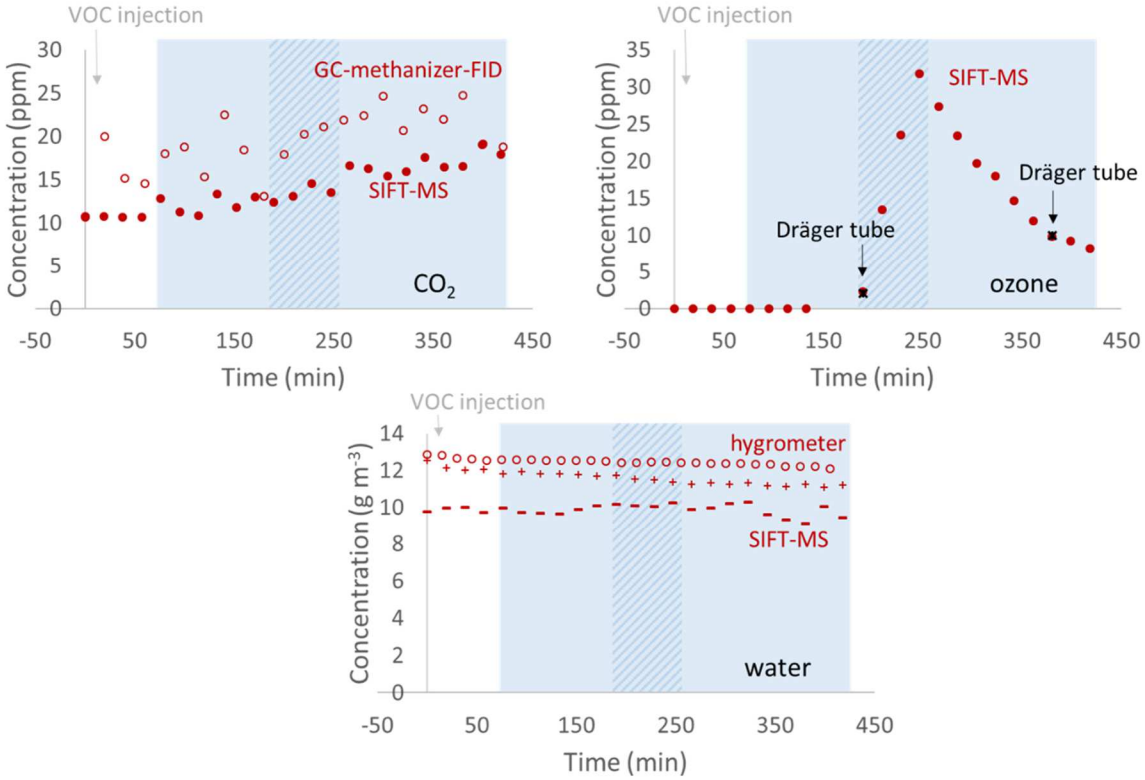

Figure 5. Monitoring over time of the concentration of: CO_2 (by SIFT-MS (●) and GC-FID (○)); ozone (SIFT-MS (●) and Dräger tubes (x)) and water (SIFT-MS in positive mode (+), in negative mode (-) and hygrometer (○)) in air in the 1.17m³ chamber during evaluation of air purifier A. Colored area: purifier ON, hatched area: ozone generation ON.

Whatever the analysis method, for device A, a clear trend is observed:

On one hand, without added VOC, a strong increase of acetaldehyde concentration is observed when ozone generation is ON, implying that it was produced by the ozone generation of the device itself (Figure 6). The same trend is also observed for formaldehyde and acetone with an increase from 14 to 184 ppbV and 4 to 65 ppbV respectively (data not shown).

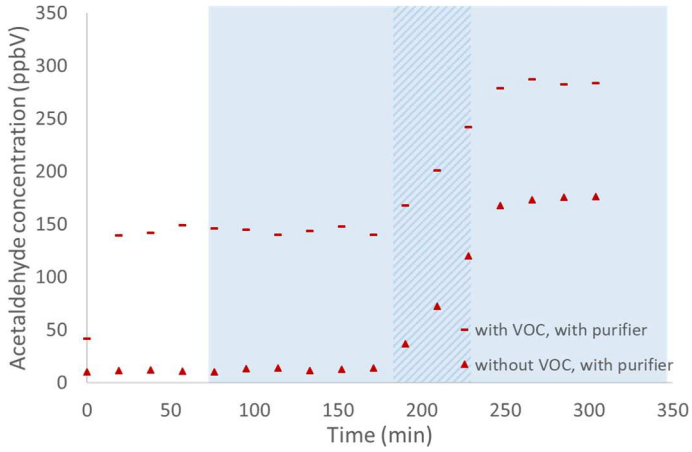

Figure 6. Monitoring over time by SIFT-MS of acetaldehyde concentrations in the 1.17 m^3 chamber during the evaluation of air purifying device A with and without VOC (including acetaldehyde) injection in the chamber. Colored area: purifier ON, hatched area: generation of ozone ON.

On the other hand, after injection of formaldehyde, its concentration regularly decreases with time up to 70% in 7 hours with the purifying device, compared to only 10% in 7 hours without any device in the test chamber. This decrease of formaldehyde seems to be only due to adsorption and no obvious influence of photocatalytic or ozone function is observed (Figure S5). Acetone concentration is stable during the experiment either with activated photocatalytic or ozone function. The concentrations of heptane and toluene are stable with only a slight decrease when the ozone function is ON. Once again, the SIFT-MS quantification of ozone is fully consistent with the control analysis with Dräger tubes. Ozone concentration sharply increases to 30 ppmV when the ozone generation is ON and slowly decreases when OFF. Ozone generation varied from 19 to 76 mg h^{-1} between two experiments for a claimed production of 50 mg h^{-1} claimed by the supplier. Carbon dioxide formation during the purifying process is not obvious, either by SIFT-MS or GC-FID/methanizer, and only a slight difference (no more than 3 ppmV) with or without added VOC may be noticed (ESI, Figure S6). This implies that VOC mineralization (oxidation to carbon dioxide) is negligible. Finally SIFT-MS analysis of water appears stable over time and its concentration using either H_3O^+ or OH^- precursor ions (10 g m^{-3}) is consistent with the value given by the hygrometry probe (13 g m^{-3}).

The results obtained with three devices are compared in Table 4. Air-purifiers B and C lead to a complete VOC elimination after 300 minutes in agreement with earlier results [39], while device A appears to be the less efficient. Indeed, this device is potentially harmful with the production of acetaldehyde and, to a lesser extent of formaldehyde and acetone, by the device itself without any added VOC. Moreover, ozone concentration detected by negative SIFT-MS during the test reached 30 ppmV after only one hour.

The main significant information brought about by SIFT-MS analysis is the simultaneous overview of ozone, carbon dioxide and water in the chamber as typically shown for air-purifier A (Figure 5). The whole set of results confirms that the calculation methods previously developed are reliable. The obvious advantage of the SIFT-MS method developed in this work is the simultaneous high frequency analysis at ppbV level of aldehydes and other VOC, in complex air matrixes containing higher level of ozone, carbon dioxide and water.

Conclusion

SIFT-MS monitoring of indoor air quality with both positive and negative ion precursors was successfully investigated in this work by single run, simultaneous analysis of the permanent air components such as oxygen, carbon dioxide and water together with volatile organic compounds and ozone. For accurate quantification of carbon dioxide, water and ozone, the formation and reactivity of hydrates of the precursor ions have to carefully considered in the calculations when using H_3O^+, OH^- or $O^{\bullet -}$ precursor ions. Reaction rate constants of all the parent precursor ions and of their hydrates, either in positive or negative ionization, were firmly established. This necessary preliminary data led to accurate concentrations of all the compounds under study with low limit of detection at the ppbV level, at least comparable or better than more conventional analysis methods based on gas chromatography. The accuracy of the SIFT-MS analysis was confirmed by comparison with other on-line analysis methods devoted to VOC (GC-FID), carbon dioxide (GC-FID/methanizer), or water (hygrometry), while high frequency analysis of aldehydes and ozone could not be carried out by alternative methods, although punctual sampling for HPLC/DNPH and Dräger tubes analysis supported very satisfactorily the SIFT-MS results.

Positive and negative SIFT-MS indoor air monitoring under standard test conditions was further used in an actual case for the evaluation of the efficiency of three air purifying devices. The simultaneous analysis of ozone, carbon dioxide and water evidenced the unsuitability and harmfulness of one of them with strong ozone and acetaldehyde release in air and negligible mineralization of VOC.

This study thus demonstrates the usefulness of positive and negative SIFT-MS for the direct, high frequency and single run analysis, without chromatographic separation, of a number of molecules such as VOC and ozone from the ppbV to the ppmV range, in complex air matrixes containing high level of water and/or carbon dioxide that are also simultaneously and continuously analyzed. This study opens the route for new original applications of this emerging technique for the monitoring of indoor air quality in the context or Sick Building Syndrome, outdoor air composition in the context of pollution peaks, and vehicles atmosphere (cars, aircrafts, trains...) for a better comfort.

References

[1] S. Karakitsios, A. Asikainen, C. Garden, S. Semple, K.D. Brouwere, K.S. Galea, A. Sánchez-Jiménez, A. Gotti, M. Jantunen, D. Sarigiannis, Integrated exposure for risk assessment in indoor environments based on a review of concentration data on airborne chemical pollutants in domestic environments in Europe, Indoor and Built Environment. 24 (2015) 1110–1146. https://doi.org/10.1177/1420326X14534865.

[2] J. Kim, S. Kim, K. Lee, D. Yoon, J. Lee, D. Ju, Indoor aldehydes concentration and emission rate of formaldehyde in libraries and private reading rooms, Atmospheric Environment. 71 (2013) 1–6. https://doi.org/10.1016/j.atmosenv.2013.01.059.

[3] M.O. Fadeyi, Ozone in indoor environments: Research progress in the past 15 years, Sustainable Cities and Society. 18 (2015) 78–94. https://doi.org/10.1016/j.scs.2015.05.011.

[4] F. Biasioli, C. Yeretzian, T.D. Märk, J. Dewulf, H. Van Langenhove, Direct-injection mass spectrometry adds the time dimension to (B)VOC analysis, TrAC Trends in Analytical Chemistry. 30 (2011) 1003–1017. https://doi.org/10.1016/j.trac.2011.04.005.

[5] D. Smith, P. Španěl, J. Herbig, J. Beauchamp, Mass spectrometry for real-time quantitative breath analysis, Journal of Breath Research. 8 (2014) 027101. https://doi.org/10.1088/1752-7155/8/2/027101.

[6] K. Sovová, K. Dryahina, P. Španěl, Selected ion flow tube (SIFT) studies of the reactions of H3O+, NO+ and O2+ with six volatile phytogenic esters, International Journal of Mass Spectrometry. 300 (2011) 31–38. https://doi.org/10.1016/j.ijms.2010.11.021.

[7] A. Gibson, L. Malek, R.F.H. Dekker, B. Ross, Detecting volatile compounds from Kraft lignin degradation in the headspace of microbial cultures by selected ion flow tube mass spectrometry (SIFT-MS), Journal of Microbiological Methods. 112 (2015) 40–45. https://doi.org/10.1016/j.mimet.2015.03.008.

[8] C. Lourenço, R. González-Méndez, F. Reich, N. Mason, C. Turner, A potential method for comparing instrumental analysis of volatile organic compounds using standards calibrated for the gas phase, International Journal of Mass Spectrometry. 419 (2017) 1–10. https://doi.org/10.1016/j.ijms.2017.05.011.

[9] V. Shestivska, M. Olšinová, K. Sovová, J. Kubišta, D. Smith, M. Cebecauer, P. Španěl, Evaluation of lipid peroxidation by the analysis of volatile aldehydes in the headspace of synthetic membranes using selected ion flow tube mass spectrometry, Rapid Communications in Mass Spectrometry. 32 (2018) 1617–1628. https://doi.org/10.1002/rcm.8212.

[10] P. Španěl, K. Dryahina, D. Smith, A general method for the calculation of absolute trace gas concentrations in air and breath from selected ion flow tube mass spectrometry data, International Journal of Mass Spectrometry. 249 (2006) 230–239. https://doi.org/10.1016/j.ijms.2005.12.024.

[11] T. Wang, P. Španěl, D. Smith, Selected ion flow tube mass spectrometry of 3-

hydroxybutyric acid, acetone and other ketones in the headspace of aqueous solution and urine, International Journal of Mass Spectrometry. 272 (2008) 78–85. https://doi.org/10.1016/j.ijms.2008.01.002.

[12] H.Z. Castada, C. Wick, K. Taylor, W.J. Harper, Analysis of Selected Volatile Organic Compounds in Split and Nonsplit Swiss Cheese Samples Using Selected-Ion Flow Tube Mass Spectrometry (SIFT-MS), Journal of Food Science. 79 (2014) C489–C498. https://doi.org/10.1111/1750-3841.12418.

[13] K. Taylor, C. Wick, H. Castada, K. Kent, W.J. Harper, Discrimination of Swiss Cheese from 5 Different Factories by High Impact Volatile Organic Compound Profiles Determined by Odor Activity Value Using Selected Ion Flow Tube Mass Spectrometry and Odor Threshold, Journal of Food Science. 78 (2013) C1509–C1515. https://doi.org/10.1111/1750-3841.12249.

[14] K. Dryahina, D. Smith, P. Španěl, Quantification of volatile compounds released by roasted coffee by selected ion flow tube mass spectrometry, Rapid Commun Mass Spectrom. 32 (2018) 739–750. https://doi.org/10.1002/rcm.8095.

[15] A. Olivares, K. Dryahina, J.L. Navarro, D. Smith, P. Španěl, M. Flores, SPME-GC-MS versus Selected Ion Flow Tube Mass Spectrometry (SIFT-MS) Analyses for the Study of Volatile Compound Generation and Oxidation Status during Dry Fermented Sausage Processing, J. Agric. Food Chem. 59 (2011) 1931–1938. https://doi.org/10.1021/jf104281a.

[16] B.J. Prince, D.B. Milligan, M.J. McEwan, Application of selected ion flow tube mass spectrometry to real-time atmospheric monitoring, Rapid Communications in Mass Spectrometry. 24 (2010) 1763–1769. https://doi.org/10.1002/rcm.4574.

[17] C. Walgraeve, K. Van Huffel, J. Bruneel, H. Van Langenhove, Evaluation of the performance of field olfactometers by selected ion flow tube mass spectrometry, Biosystems Engineering. 137 (2015) 84–94. https://doi.org/10.1016/j.biosystemseng.2015.07.007.

[18] A. Knížek, K. Dryahina, P. Španěl, P. Kubelík, L. Kavan, M. Zukalová, M. Ferus, S. Civiš, Comparative SIFT-MS, GC–MS and FTIR analysis of methane fuel produced in biogas stations and in artificial photosynthesis over acidic anatase TiO2 and montmorillonite, Journal of Molecular Spectroscopy. 348 (2018) 152–160. https://doi.org/10.1016/j.jms.2017.10.002.

[19] E. Michel, N. Schoon, C. Amelynck, C. Guimbaud, V. Catoire, E. Arijs, A selected ion flow tube study of the reactions of H3O+, NO+ and O2+ with methyl vinyl ketone and some atmospherically important aldehydes, International Journal of Mass Spectrometry. 244 (2005) 50–59. https://doi.org/10.1016/j.ijms.2005.04.005.

[20] M. Ghislain, N. Costarramone, J.-M. Sotiropoulos, T. Pigot, R.V.D. Berg, S. Lacombe, M.L. Bechec, Direct analysis of aldehydes and carboxylic acids in the gas phase by negative ionization SIFT-MS: quantification and modeling of ion-molecule reactions, Rapid Communications in Mass Spectrometry. 0 (n.d.). https://doi.org/10.1002/rcm.8504.

[21] P. Harb, L. Sivachandiran, V. Gaudion, F. Thevenet, N. Locoge, The 40 m 3 Innovative experimental Room for INdoor Air studies (IRINA): Development and validations, Chemical

Engineering Journal. 306 (2016) 568–578. https://doi.org/10.1016/j.cej.2016.07.102.

[22] D. Smith, P. Španěl, Selected ion flow tube mass spectrometry (SIFT-MS) for on-line trace gas analysis, Mass Spectrom. Rev. 24 (2005) 661–700. https://doi.org/10.1002/mas.20033.

[23] D. Smith, P. Španěl, SIFT-MS and FA-MS methods for ambient gas phase analysis: developments and applications in the UK, The Analyst. 140 (2015) 2573–2591. https://doi.org/10.1039/C4AN02049A.

[24] D. Hera, V. Langford, M. McEwan, T. McKellar, D. Milligan, Negative Reagent Ions for Real Time Detection Using SIFT-MS, Environments. 4 (2017) 16. https://doi.org/10.3390/environments4010016.

[25] P. Španěl, D. Smith, T.A. Holland, W.A. Singary, J.B. Elder, Analysis of formaldehyde in the headspace of urine from bladder and prostate cancer patients using selected ion flow tube mass spectrometry, Rapid Communications in Mass Spectrometry. 13 (1999) 1354–1359. https://doi.org/10.1002/(SICI)1097-0231(19990730)13:14<1354::AID-RCM641>3.0.CO;2-J.

[26] P. Španěl, D. Smith, Progress in SIFT-MS: Breath analysis and other applications, Mass Spectrom. Rev. 30 (2011) 236–267. https://doi.org/10.1002/mas.20303.

[27] L. Vitola Pasetto, V. Simon, R. Richard, J.-S. Pic, F. Violleau, M.-H. Manero, Aldehydes gas ozonation monitoring: Interest of SIFT/MS versus GC/FID, Chemosphere. 235 (2019) 1107–1115. https://doi.org/10.1016/j.chemosphere.2019.06.186.

[28] P. Spanel, D. Smith, Influence of water vapour on selected ion flow tube mass spectrometric analyses of trace gases in humid air and breath, Rapid Communications in Mass Spectrometry. 14 (2000) 1898–1906. https://doi.org/10.1002/1097-0231(20001030)14:20<1898::AID-RCM110>3.0.CO;2-G.

[29] A. Spesyvyi, D. Smith, P. Spanel, Ion chemistry at elevated ion-molecule interaction energies in a selected ion flow-drift tube: reactions of H3O+, NO+ and O2+ with saturated aliphatic ketones, Physical Chemistry Chemical Physics. (2017). https://doi.org/10.1039/C7CP05795D.

[30] S. Williams, M.F. Campos, A.J. Midey, S.T. Arnold, R.A. Morris, A.A. Viggiano, Negative Ion Chemistry of Ozone in the Gas Phase, J. Phys. Chem. A. 106 (2002) 997–1003. https://doi.org/10.1021/jp012929r.

[31] P. Španěl, D. Smith, On-line measurement of the absolute humidity of air, breath and liquid headspace samples by selected ion flow tube mass spectrometry, Rapid Communications in Mass Spectrometry. 15 (2001) 563–569. https://doi.org/10.1002/rcm.265.

[32] J. Rodier, B. Legube, R. Brunet, Ozone. In L'analyse de l'eau, 9ème édition, Eaux naturelles, eaux résiduaires, eau de mer., Dunod, Dunod, Paris, 2009.

[33] NF EN 16846-1 - Photocatalysis - Measurement of efficiency of photocatalytic devices

used for the elimination of VOC and odour in indoor air in active mode - Part 1: Batch mode test method in closed chamber, (2017). https://www.boutique.afnor.org/norme/nf-en-16846-1/photocatalyse-mesure-de-l-efficacite-des-dispositifs-photocatalytiques-servant-a-l-elimination-en-mode-actif-des-cov-et-des-odeu/article/823482/fa185277 (accessed August 22, 2019).

[34] N. Costarramone, C. Cantau, V. Desauziers, C. Pecheyran, T. Pigot, S. Lacombe, Photocatalytic air purifiers for indoor air: European standard and pilot room experiments, ENVIRONMENTAL SCIENCE AND POLLUTION RESEARCH. 24 (2017) 12538–12546. https://doi.org/10.1007/s11356-016-7607-z.

[35] P. Spanel, D. Smith, Reactions of Hydrated Hydronium Ions and Hydrated Hydroxide Ions with Some Hydrocarbons and Oxygen-Bearing Organic Molecules, J. Phys. Chem. 99 (1995) 15551–15556. https://doi.org/10.1021/j100042a033.

[36] A.B. Raksit, D.K. Bohme, An experimental study of the influence of hydration on the reactivity of the hydroxide anion in the gas phase at room temperature, Can. J. Chem. 61 (1983) 1683–1689. https://doi.org/10.1139/v83-287.

[37] S.T. Arnold, A.A. Viggiano, R.A. Morris, Rate Constants and Product Branching Fractions for the Reactions of H_3O^+ and NO^+ with C_2-C_{12} Alkanes, The Journal of Physical Chemistry A. 102 (1998) 8881–8887. https://doi.org/10.1021/jp9815457.

[38] P. Španěl, D. Smith, AccountOn the features, successes and challenges of selected ion flow tube mass spectrometry, European Journal of Mass Spectrometry. 19 (2013) 225. https://doi.org/10.1255/ejms.1240.

[39] N. Costarramone, B. Kartheuser, C. Pecheyran, T. Pigot, S. Lacombe, Efficiency and harmfulness of air-purifying photocatalytic commercial devices: From standardized chamber tests to nanoparticles release, Catalysis Today. 252 (2015) 35–40. https://doi.org/10.1016/j.cattod.2015.01.008.

Table 1. Product ions obtained by reaction between the permanent components of an air matrix (oxygen, water, carbon dioxide) and the eight listed reagent ions.

Reacting molecule	**H_3O^+**		**$O_2^{\bullet+}$**		**NO^+**		**OH^-**		**$O^{\bullet-}$**		**$O_2^{\bullet-}$**		**NO_2^-**		**NO_3^-**	
	ion	***m/z***	**ion**	***m/z***	**Ion**	***m/z***	**ion**	***m/z***	**ion**	***m/z***	**ion**	***m/z***	**ion**	***m/z***	**ion**	***m/z***
	H_3O^+	19	$O_2^{\bullet+}$	32	NO^+	30	OH^-	17	$O^{\bullet-}$	16	$O_2^{\bullet-}$	32	NO_2	46	NO_3^-	62
water	**$H_3O^+.H_2O$**	37			$NO^+.H_2O$	48	$OH^-.H_2O$	35	OH^-	17	$O_2^{\bullet-}.H_2O$	50				
water	**$H_3O^+.(H_2O)_2$**	55					$OH^-.(H_2O)_2$	53	$OH^-.H_2O$	35						
water	**$H_3O^+.(H_2O)_3$**	73							$OH^-.(H_2O)_2$	53						
O_2							$O_2^{\bullet-}$	32 (93) [a]	$O_2^{\bullet-}$ (13) [a]	32	$O_3^{\bullet-}$	48				
O_2							$O_3^{\bullet-}$	48 (7) [a]	$O_3^{\bullet-}$ (87) [a]	48						
CO_2							$CO_2.O^{\bullet-}$	60	$CO_2.O^{\bullet-}$	60	$CO_2.O_2^{\bullet-}$	76				
CO_2							HCO_3^-	61	HCO_3^-	61						
CO_2							$CO_2.O_2^{\bullet-}$	76	$CO_2.O_2^{\bullet-}$	76						
CO_2							$HCO_3^-.H_2O$	79	$HCO_3^-.H_2O$	79						

[a] Number between brackets are the intensity ratio

Table 2. Experimental (k) rate constants (in $cm^3\ s^{-1}$) for the primary reactions of the matrix components with the different reagent ions. In the case of three-body reactions, rate constant in this table correspond to the effective bimolecular rate constant (k) under the experimental conditions of this work.

	H_3O^+	**$O_2^{\bullet+}$**	**NO^+**	**OH^-**	**$O^{\bullet-}$**	**$O_2^{\bullet-}$**	**NO_2^-**	**NO_3^-**
Water	$7.16\ 10^{-11}$	/	$6.08\ 10^{-13}$	$1.06\ 10^{-12}$	$1.32\ 10^{-12}$	$7.73\ 10^{-13}$	/	/
Carbon dioxide	/	/	/	$2.92\ 10^{-12}$	ND	$2.63\ 10^{-13}$	/	/
Dioxygen	/	/	/	$1.50\ 10^{-11}$	ND	$1.04\ 10^{-12}$	/	/

ND: not determined due to OH^- precursor ion present even without added water in the flow tube (arising from the plasma discharge).

Table 3. Product ions between VOC and the six positive and negative precursor ions used in SIFT-MS. Both primary (in bold) and secondary (in italic) ion products are listed. In brackets, m/z.

	H_3O^+	$O_2^{\bullet+}$	NO^+	OH^-	$O^{\bullet-}$	$O_2^{\bullet-}$
Formaldehyde	**$HCHOH^+$ (31)** *$HCHO.HCHOH^+$ (61)* *$HCHOH^+.H_2O$ (49)*	**HCO^+ (29)** **$HCHO^{\bullet+}$ (30)**	-	**HCO^- (29)** *$HCHO.HCO^-$ (59)* *$HCO^-.H_2O$ (47)*	**HCO^- (29)** *$HCHO.HCO^-$ (59)* *$HCO^-.H_2O$ (47)*	**HCO^- (29)** *$HCHO.HCO^-$ (59)* *$HCO^-.H_2O$ (47)*
Acetaldehyde	**CH_3CHOH^+ (45)** *$CH_3CHO.CH_3CHOH^+$ (89)* *$CH_3CHOH^+.H_2O$ (63)*	**CH_2CHO^+ (43)** **$CH_3CHO^{\bullet+}$ (44)** *$CH_3CHO.CH_3CHOH^+$ (89)*	**CH_2CHO^+ (43)**	**CH_2CHO^- (43)** *$CH_3CHO.CH_2CHO^-$ (87)* *$CH_2CHO^-.H_2O$ (61)*	**CH_2CHO^- (43)** *$CH_3CHO.CH_2CHO^-$ (87)* *$CH_2CHO^-.H_2O$ (61)*	**CH_2CHO^- (43)** *$CH_3CHO.CH_2CHO^-$ (87)* *$CH_2CHO^-.H_2O$ (61)*
Acetone	**$CH_3COCH_3H^+$ (59)** $CH_3COCH_3.CH_3COCH_3H^+$ (117) $CH_3COCH_3H^+.H_2O$ (77)	**$CH_3COCH_3^{\bullet+}$ (58)** **CH_3CO^+ (43)**	**$CH_3COCH_3.NO^+$ (88)**	**$CH_3COCH_2^-$ (57)** *$CH_3COCH_2^-.H_2O$ (75)*	**$CH_3COCH_2^-$ (57)** *$CH_3COCH_2^-.H_2O$ (75)*	**$CH_3COCH_2^-$ (57)** *$CH_3COCH_2^-.H_2O$ (75)*
Toluene	**$C_7H_9^+$ (93)**	**$C_7H_8^{\bullet+}$ (92)**	**$C_7H_8^{\bullet+}$ (92)**	**$C_7H_7^-$ (91)**	**$C_7H_7^-$ (91)**	**$C_7H_7^-$ (91)**
Heptane	**$C_4H_9^+$ (57)**	**$C_7H_{16}^{\bullet+}$ (100)** **$C_5H_{11}^+$ (71)** **$C_4H_9^+$ (57)**	**$C_7H_{15}^+$ (99)**	-	-	-

Table 4. Elimination rate (%) of the 5 VOC with the 3 different air purifiers after 300 min.

		Elimination rate (%)		
	Without purifier	Purifier A	Purifier B	Purifier C
Formaldehyde	10	66	98	99
Acetaldehyde	30	Production: +83%	96	96
Acetone	11	5	96	97
Heptane	10	23	> 99	> 99
Toluene	12	19	> 99	> 99